Orbit Determination for Asteroid 2102 Tantalus

(27 July 2014)

David Rower[1], Joey Li[1], and Saanya Jain[1]

[1]Summer Science Program, Santa Barbara, CA USA

***Abstract*—The precise tracking and determination of near-earth asteroid orbits is of importance to the scientific community due to the possible danger that such objects impose. 2102 Tantalus is one such asteroid, which was imaged and analyzed using multiple sets of data collected from three different locations over a one month period. Using a least-squares plate reduction to determine the right ascension and declination of the asteroid during each observation, the orbital elements were determined, creating the possibility of a long-term integration of the asteroid's orbit to check for the possibility of a future collision with Earth. The results for the orbital elements obtained were a semi-major axis a of 1.26 AU $\pm$ 0.12 AU, an eccentricity e of 0.306 $\pm$ 0.020°, an inclination angle i of 62° $\pm$ 5.1°, a longitude of ascending node Ω of 94.9° $\pm$ 1.8°, an argument of perihelion ω of 60° $\pm$ 15°, and a time at last perihelion (T) of 2456690 JD $\pm$ 16 JD.**

***Keywords*—2102 Tantalus, orbit determination, near-earth, asteroid, Keplerian, orbital elements, potentially hazardous asteroid, PHA**

I. Introduction

There are several benefits to tracking and analyzing the orbit of near-earth asteroids, though the primary motivation for this project was the danger of the proximity of 2102 Tantalus' orbit. Much research is needed to keep track of an asteroid's orbit because, though an orbit may seem stable during a given period, perturbations by massive bodies in the solar system may shift the orbit to a collision trajectory.

Another one of the benefits of researching near-earth asteroids is the possibility of scientific research. The Asteroid Redirect Mission proposed to NASA depends on the capture of a near-earth asteroid in order to manipulate its orbit, stop a collision trajectory, or even bring the body into an orbit around the moon, creating the possibility of hands-on research. This mission needs target bodies that are within a reasonable range, and that are also well-documented and observed.

2102 Tantalus was imaged using three different telescopes: a 14" Meade telescope and a 24" Keck telescope, both at the campus of Westmont College, CA, and the Cerro Tololo Observatory in Chile using the Panchromatic Robotic Optical Monitoring and Polarimetry Telescopes. Kepler's laws of planetary motion were used to derive an equation of the orbit, and the Method of Gauss was then used to determine the orbital elements through a series of converging iterations. The uncertainty in these elements should be acknowledged due to the simplification of the model of the orbit. The force of gravity due to the sun was the only force used in the calculations, and so no perturbations were accounted for.

II. Methods

A. Telescopes

These are the specifcations for the three telescopes used:

Telescope	Field of View	Lat, Long	Primary Mirror	Observatory Code
Keck	17" x 17"	latitude: 34°26'44.01" longitude: -119°39'42.01"	0.6 m	G60
Meade	20" x 16"	latitude: 34°26'44.01" longitude: -119°39'42.01"	14 in.	G60
Prompt 1	10" x 10"	latitude: -30°10'03.50" longitude: -70°48'19.40"	0.41m	807
Prompt 2	21" x 14"	latitude: -30°10'03.50" longitude: -70°48'19.40"	0.41m	807
Prompt 8	23" x 23"	latitude: -30°10'03.50" longitude: -70°48'19.40"	0.41m	807

TABLE I: This table includes the specifications of each telescope used, including name, field of view, latitude and longitude of its location, size of dish, and observatory code

B. Observation Procedures

Before each observation session, the JPL Horizons Database was used to find the expected right ascension (RA) and declination of 2102 Tantalus. Using the predicted RA and Local Sidereal Time, the Hour Angle of the asteroid was calculated. The Hour Angle was used as a rough approximation of the asteroid's position, and after looking at the location in the sky, a bright star within 30° RA and declination of 2102 Tantalus was chosen to sync CCDSoft, the telescope tracking software, with SkyX, the star database software.

The telescope was then slewed to the RA and Declination of 2102 Tantalus. In order to focus the telescope, continuous images of a sub-frame with 1x1 binning and a two to five second exposure were taken, adjusting the focus until the

images were clear. Well defined and symmetric stars were the criteria for a focused image.

Before taking sets to be used in the orbit determination, reference stars in the image frame were confirmed to resemble the those in the finder chart and the SkyX software. Images with 2x2 binning of 10-30 second exposures were then taken in staggered intervals of ten minutes.

For the Chilean telescopes, the Skynet telescope interface was used to request observations. Filters, exposure times, number of exposures, and delay between exposures were specified and used in the data acquisition.

C. Data Analysis

Two programs were used in the data analysis, the first of which calculated the centroids of the reference stars, and the second of which used a least-squares plate reduction to determine the RA and declination of the asteroid.

1) Centroid: This program read in a .fit image, and used an aperture with a size specified by the user, according to how large the bright object appeared, to find the center of the bright object through a weighted average. These centroids were then used as inputs for the least-squares plate reduction (LSPR) program.

2) LSPR: This program read in a text file which included the centroids of the reference stars and asteroid, as well as the right ascension and declination of each reference star. The program then calculated a best-fit line through a least-squares plate reduction model in order to determine the relationship between the array of the .fit image and the right ascencion and declination of the objects in the image. The program output was the right ascension and declination of the asteroid.

The RA and declination obtained from the LSPR program was run through our orbital element determination (OD) program, which returned the six Keplerian orbital elements. The uncertainty of the orbital elements were then calculated, and were compared to the values found in the JPL Small-Body Database.

3) Orbital Element: With the RA and declination from three observations and adjusting for parallax, the Method of Gauss can be used to determine the position $\mathbf{r}$ and $\dot{\mathbf{r}}$ vectors, which can be used to calculate the orbital elements

Calculations With the Gaussian Method Once the right ascension and declination for the five observations have been calculated, it was possible to proceed with the orbit determination, using a method originally developed by Gauss. The data from three observations was used. let ρ be the vector from the Earth to the asteroid, $\mathbf{R}$ be the vector from the Earth to the Sun, and $\mathbf{r}$ be the vector from the Sun to the asteroid (see figure 1). Vector algebra shows that

$$\boldsymbol{\rho} = \mathbf{R} + \mathbf{r}. \tag{1}$$

The direction to the asteroid from the Earth can be determined using the right ascension and declination, but the distance to it is unknown. As a result it is helpful to write the equation as

$$\rho\hat{\rho} = \mathbf{r} + \mathbf{R}. \tag{2}$$

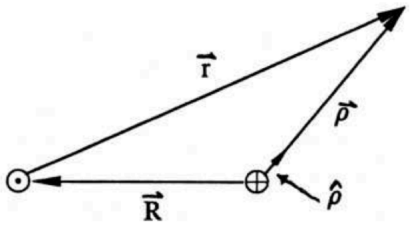

Fig. 1: The vectors between the Earth, Sun, and asteroid

If the range to the asteroid, ρ, is known, then is is possible to solve for the position of the asteroid.

$$\mathbf{r} = \rho\hat{\rho} - \mathbf{R}. \tag{3}$$

Gauss' method involves using a series of approximations to find the range and hence the orbit of the asteroid. For the problem of orbit determination, it is often helpful to used modified time, defined by

$$\tau = k(t - t_2). \tag{4}$$

in which t_2 is the time of the second observation.

Since the orbit is being approximated as a two-body orbit, the potential is simply that of the attractive inverse square field. Given the potential, we can derive the equations of motion. According to Hamiltons' equations of classical mechanics, it is possible to completely determine the motion of a system given an initial position and velocity. r can be expressed as a function of time as

$$\mathbf{r}(\tau) = f\mathbf{r}_2 + g\dot{\mathbf{r}}_2 \tag{5}$$

To find f and g, we first start with the general power series expansion for $\mathbf{r}$. As with time, we take the second observation as the the standard and center the series about $\mathbf{r}_2$.

$$\mathbf{r}(\tau) = \mathbf{r}_2 + \dot{\mathbf{r}}_2\tau + \frac{1}{2!}\ddot{\mathbf{r}}\tau^2 + \cdots \tag{6}$$

Newton's law of gravitation, in the present notation, reads

$$\ddot{\mathbf{r}} = -\frac{\mu}{\mathbf{r}^3}\mathbf{r}, \tag{7}$$

in which the parameter μ equals one when measured in solar masses. This gives the second derivative of $\mathbf{r}$ in terms of $\mathbf{r}$. Since the third derivative can be expressed as the derivative of the second derivative, and so on ad infinitum, it becomes possible to express the entire series of $\mathbf{r}$ in terms of $\mathbf{r}$ and $\dot{\mathbf{r}}$, justifying (5). Working through the derivatives gives

$$f = 1 - \frac{1}{2r_2^3}\tau^2 + \frac{\mathbf{r}_2 \cdot \dot{\mathbf{r}}_2}{2r_2^5}\tau^3 + \cdots \tag{8}$$

$$g = \tau - \frac{1}{6r_0^3}\tau^3 + \frac{\mathbf{r}_2 \cdot \dot{\mathbf{r}}_2}{4r_0^5}\tau^4 + \cdots \tag{9}$$

τ_2 is zero, but using τ_1 and τ_3 in (6) gives

$$\mathbf{r}_1 = f_1\mathbf{r}_2 + g_1\dot{\mathbf{r}}_2 \tag{10}$$

$$\mathbf{r}_3 = f_3\mathbf{r}_2 + g_3\dot{\mathbf{r}}_2 \tag{11}$$

(10) and (11) combine to give

$$\dot{\mathbf{r}}_2 = \frac{f_3}{g_1f_3 - g_3f_1}\mathbf{r}_1 - \frac{f_1}{g_1f_3 - g_3f_1}\mathbf{r}_3 \tag{12}$$

By writing (3) in terms of all the components and taking dot and cross products, it is possible to eliminate two of three components of ρ. In other words, it is possible to derive expressions for ρ_1, ρ_2, and ρ_3 in terms of the f and g series, the $\mathbf{R}$ vectors, and the components of $\hat{\rho}$.

However, the f and g series depend on $\mathbf{r}$ and $\dot{\mathbf{r}}$. The initial estimate of $\mathbf{r} = (1.4, 0, 0)$ $\dot{\mathbf{r}} = (0, 0, 0)$ and was used, and then $\mathbf{r}$ was recalculated, and $\dot{\mathbf{r}}$ redetermined using (12). This process was repeated until the values of $\mathbf{r}$ converged, usually after about twenty iterations.

After obtaining values for $\mathbf{r}$ and $\dot{\mathbf{r}}$ in equatorial coordinates, they were converted to ecliptic coordinates by rotating it around the x-axis by $-\epsilon$, in which $\epsilon = 23.43741°$, the inclination of the rotation of the Earth during the times of observation.

Using $\mathbf{r}$ and $\dot{\mathbf{r}}$, we can now calculate the 6 orbital elements using the following equations:

Orbital Elements	**Description**
a (AU)	semi-major axis
e	eccentricity
i (degrees)	inclination
Ω (degrees)	longitude of ascending node
ω (degrees)	argument of perihelion
T (JD)	time of last perihelion

TABLE II: Classical Orbital Elements

semi-major axis:	half of the distance from the center to the furthest point in the orbit
eccentricity:	a measure of how much the orbit deviates from a circular orbit
inclination:	the angle between the orbital plane and the ecliptical plane
longitude of ascending node:	the angle from the vernal equinox to the point where the object crosses the ecliptic traveling from south to north
argument of perihelion:	angle between the ascending node and perihelion
time of last perihelion:	Julian day on which perihelion last occurred

TABLE III: Glossary of Orbital Elements

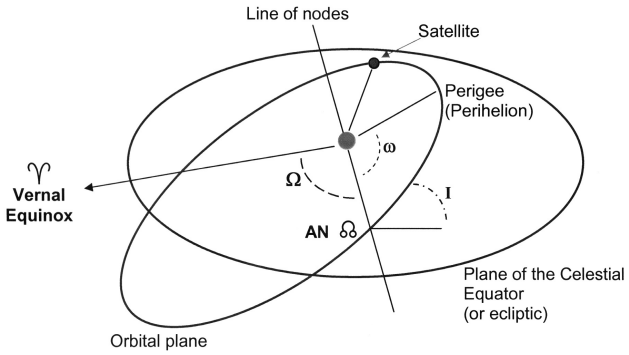

Fig. 2: Orbital Elements

First, the eccentricity (**e**) vector needs to be calculated:

$$\mathbf{e} = \frac{\mathbf{r}_2 \times \mathbf{h}}{\mu} - \frac{\mathbf{r}_2}{r_2} \tag{13}$$

Second, the angular momentum (**h**) vector:

$$\mathbf{h} = \mathbf{r}_2 \times \dot{\mathbf{r}}_2 \tag{14}$$

Third, the node vector **N**):

$$\mathbf{N} = \hat{z} \times \mathbf{h} \tag{15}$$

Now, to calculate the orbital elements:
where

$$v = |\dot{\mathbf{r}}| \tag{16}$$

and μ = 1
a:

$$\frac{1}{a} = \frac{2}{r} - \frac{v^2}{\mu} \tag{17}$$

i:

$$\cos i = \frac{\mathbf{h}\hat{z}}{h} \tag{18}$$

Ω:

$$\cos \Omega = \frac{N_x}{|\mathbf{N}|} \tag{19}$$

ω:

$$\cos \omega = \frac{\mathbf{N} \cdot \mathbf{e}}{|\mathbf{N}||\mathbf{e}|} \tag{20}$$

T:

$$T = t - \frac{M}{n} \tag{21}$$

n:

$$n = k\sqrt{\frac{\mu}{a^3}} \tag{22}$$

D. Calculations and Uncertainty

To calculate the reported classical orbital elements and their uncertainties, the "jackknife" method was used. While Gauss' method finds the orbital elements from only three observations, data from seven independent observations were pooled together and used in the orbit determination. Using every possible combination of all observations, there are a total of $\binom{7}{3} = 35$ different sets to calculate the orbital elements with.

Gauss' method was performed 35 times, with the values of the orbital elements for each combination stored in arrays. The final values of the elements were calculated by taking the mean of the values, with the uncertainties being defined as their standard deviations. The classical orbital elements and their uncertainties are shown in Table III.

Ephemeris Generation Check: To verify that the data is correct, the classical orbital elements were entered into an ephemeris generation program, which used them to solve for the right ascension and declination. Table IV shows a comparison of calculated and observed values.

III. Data

The images used along with data tables including the information for their respective 8 reference stars are included in the Appendix.

The calculated orbital elements are in table IV, and the comparisons with the previously accepted values are in table V.

Orbital Element	Value	Uncertainty
a (AU)	1.29	0.0155
e	0.299	0.00366
i (degrees)	64.1	0.330
Ω (degrees)	94.3	0.126
ω (degrees)	62	1.83
T (JD)	2456684	3.67
M (degrees)	76	5.10

TABLE IV: Classical orbital elements and their uncertainties (one standard deviation)

Orbital Elements	Calculated Value	JPL Value	Difference
a (AU)	1.29	1.29004040	0.00313%
e	0.299	0.29907421	0.0248%
i (degrees)	64.1	64.00771819	0.144%
Ω (degrees)	94.3	94.38021630	0.0849%
ω (degrees)	62	61.57439361	0.686%
T (JD)	2456684	2456737.76819	0.00219%
M (degree)	76.31	42.19751642	44.7%

TABLE V: Comparison of calculated data with accepted values obtained from JPL Horizons.

IV. Results/Discussion

The calculated orbital elements of 2102 Tantalus (Table IV) have an inherent degree of uncertainty. We used the second, third and fourth observations from Table V, and the orbit determined using those measurements predict the RA and Dec of the asteroid during the first observation well (Table VI). The values according to the JPL database of the orbital elements are located within the uncertainty of the measurements from this data (Table VII), and so the measurements are consistent with previous measurements, although several sources of error contributed to the uncertainty of the results. Some of the sources of error can be classified as systematic; systematic errors can be attributed to the precision (or lack thereof) of the telescopes, software, and methods used to gather data and arrive at the orbital elements. The centroid program relied on an aperture which was in the shape of a square, however, this shape may not have been optimal for finding the centroid of each reference star. The LSPR program approximated the curvature of space to be a flat plane, though this approximation is most likely negligible due to the low declination of 2102 Tantalus. Both the Centroid and LSPR programs were written in python, and floating point errors propagated through numerous calculations, possibly magnifying a negligible error to a

significant level. Other sources of error can be classified as random; in measuring the centroid of each reference star, the wrong pixel may have been chosen as the closest to the center, and the streaking of the asteroid in certain photos may have led to the calculation of a false right ascension and declination for a certain observation.

As previously mentioned, the method of "jackknifing" was used in order to calculate the standard deviation of the orbital elements. This practice violates the assumption that all observations used to calculate the error are independent, and so this method does not yield an accurate uncertainty. This should be acknowledged when viewing the uncertainties.

The apparent magnitude of the asteroid during each observation was also calculated (Table VIII).

**All tables located in Appendix*

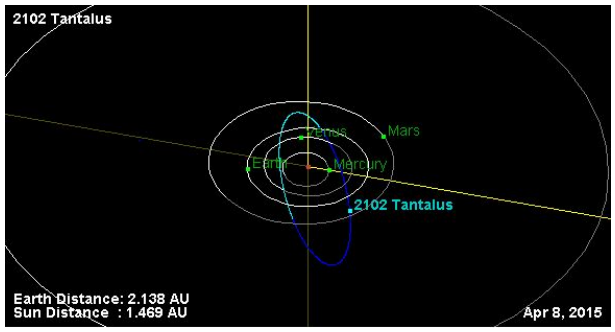

Fig. 3: Visualisation of Tantalus's orbit from JPL's database

V. Conclusion

Using data from seven independent observations, the orbital elements of 2102 Tantalus were calculated. Eight reference stars were chosen in each observation, and the centroids of those reference stars were then calculated. These centroids and known stars' right ascensions and declinations were used to conduct a least-squares plate reduction, which allowed the right ascension and declination of 2102 Tantalus to be determined. Using the calculated RA and Dec for each observation, the orbital elements of the asteroid were determined, and compared to those provided by the JPL Database.

The orbital elements were calculated from the mean of all 35 combinations of the independent observations, and this method ("jackknifing") may have yielded inaccurate elements and false uncertainties. The largest difference in values was from the inclination, which has a 3.14% difference from the JPL Database value. Improvement of the calculated orbital elements could be achieved through taking more independent observations of the asteroid, using the equipment during the observations more precisely, and also by using more precise equipment.

The nature of 2102 Tantalus' as well as other near-earth asteroids' orbits makes more precise observations important in terms of assuring the safety of earth from the improbable, but not impossible, event of a collision.

Appendix A
Images and Reference Stars

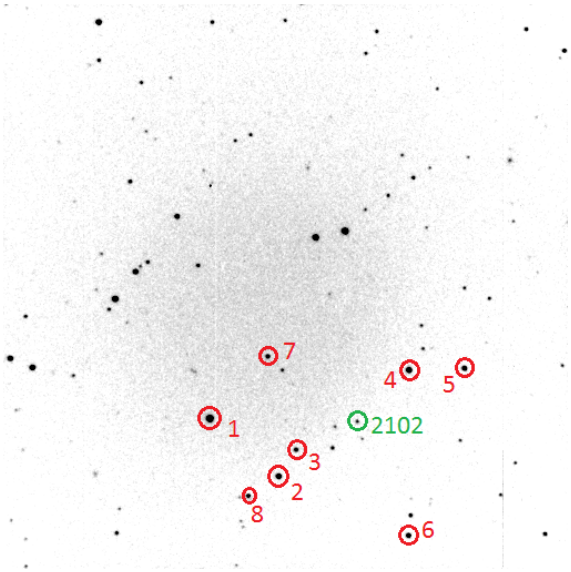

Fig. 4: Asteroid image taken on 4 July 2014 08:36:56.21UT. Exposure length: 10s. JD: 2456842.858333 Binning: 1x1

Star	RA	DEC	X of pixel	Y of pixel	Residuals
1: UCAC3 222:117962	15h 38m 50.26s	20°41' 17.49"	187.955	374.909	RA:0.185s DEC:-0.303"
2: UCAC3 222:117955	15h 38m 42.17s	20°39' 21.84"	249.977	426.980	RA:0.416s DEC:-0.228"
3: UCAC3 222:117953	15h 38m 39.62s	20°40' 06.15"	265.969	403.925	RA:0.985s DEC:1.318"
4: UCAC3 222:117935	15h 38m 24.11s	20°42' 09.54"	367.093	331.042	RA:-1.127s DEC:-0.613"
5: UCAC3 222:117927	15h 38m 17.00s	20°42' 02.58"	417.906	329.947	RA:0.788s DEC:0.158"
6: UCAC3 222:117940	15h 38m 26.23s	20°37' 11.87"	366.986	480.912	RA:-0.241s DEC:-0.047"
7: UCAC3 222:117954	15h 38m 42.07s	20°42' 59.07"	239.998	319.003	RA:-0.253s DEC:0.169"
8: UCAC3 222:117960	15h 38m 46.31s	20°38' 51.21"	222.033	444.997	RA:-0.754s DEC:-0.453"

TABLE VI: The reference stars used in Figure 4

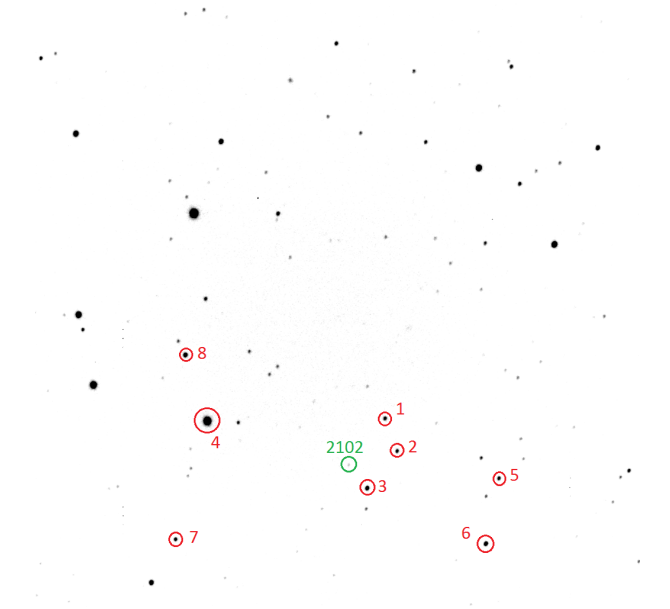

Fig. 5: Asteroid image taken on 17 July 2014 05:22:27.28 UT. Exposure length: 10s. JD: 2456855.7 Binning 1x1

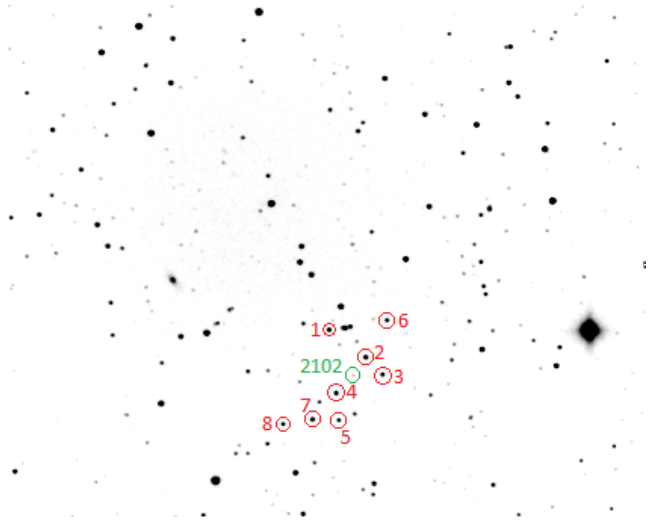

Fig. 6: Asteroid image taken on 21 July 2014 05:28:35.16 UT. Exposure length: 30s. JD: 2456859.7 Binning 3x3

Star	RA	DEC	X of pixel	Y of pixel	Residuals
1: UCAC3 168:136971	15h 11m 59.90s	-6°27' 44.54"	592.962	703.011	RA:0.402s DEC:0.482"
2: UCAC3 168:136969	15h 11m 58.89s	-6°28' 41.58"	613.028	758.028	RA:-0.064s DEC:0.180"
3: UCAC3 168:136976	15h 12m 02.68s	-6°29' 39.22"	561.529	819.612	RA:-1.035s DEC:-1.064"
4: UCAC3 168:136951	15h 12m 20.05s	-6°27' 19.37"	291.544	706.396	RA:-0.311s DEC:0.020"
5: UCAC3 167:136899	15h 11m 47.66s	-6°29' 44.47"	785.867	804.052	RA:0.448s DEC:-0.228"
6: UCAC3 168:137010	15h 11m 49.89s	-6°31' 32.08"	763.042	914.944	RA:-0.028s DEC:0.438"
7: UCAC3 168:137008	15h 12m 24.95s	-6°30' 34.04"	238.971	907.067	RA:0.479s DEC:0.202"
8: UCAC3 167:136958	15h 12m 21.82s	-6°25' 24.46"	254.461	594.580	RA:0.109s DEC:-0.030"

TABLE VII: The reference stars used in Figure 5

Star	RA	DEC	X of pixel	Y of pixel	Residuals
1: UCAC3 156:142663	15h 8m 40.33s	-12°2' 02.38"	215.997	216.012	RA:0.582s DEC:0.785"
2: UCAC3 156:142650	15h 8m 35.97s	-12°3' 03.94"	240.018	234.021	RA:-0.459s DEC:-0.978"
3: UCAC3 156:142647	15h 8m 34.10s	-12°3' 41.08"	251.010	245.982	RA:-0.440s DEC:0.009"
4: UCAC3 156:142664	15h 8m 40.46s	-12°4' 05.61"	220.984	257.997	RA:1.688s DEC:0.642"
5: UCAC3 156:142665	15h 8m 40.57s	-12°4' 58.09"	222.017	275.993	RA:-0.292s DEC:0.568"
6: UCAC3 156:142642	15h 8m 32.61s	-12°1' 58.20"	254.008	209.992	RA:-0.554s DEC:-0.296"
7: UCAC3 156:142670	15h 8m 44.00s	-12°4' 50.15"	204.998	275.015	RA:1.184s DEC:0.235
8: UCAC3 156:142677	15h 8m 47.91s	-12°4' 51.98"	184.503	277.499	RA:-1.710s DEC:-0.965"

TABLE VIII: The reference stars used in Figure 6

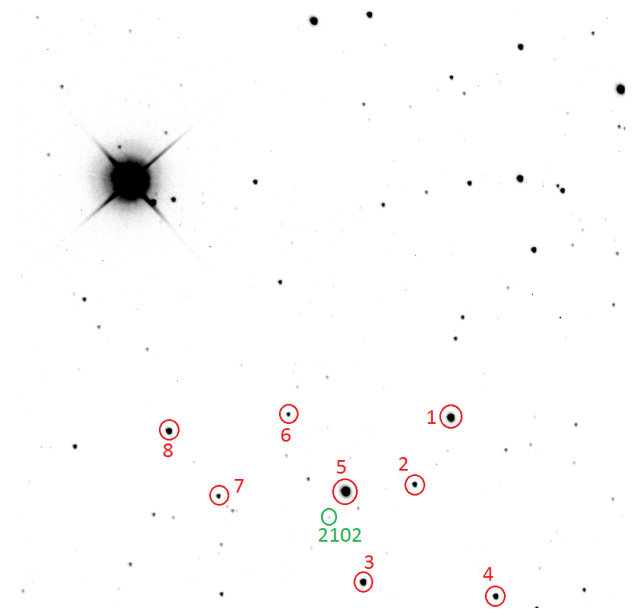

Fig. 7: Asteroid image taken on 25 July 2014 01:01:55 UT. Exposure length: 20s. JD: 2456863.5 Binning 3x3

Star	RA	DEC	X of pixel	Y of pixel	Residuals
1: UCAC3 147:146940	15h 6m 26.84s	-16°32' 30.73"	726.097	701.556	RA:0.081s DEC:0.016"
2: UCAC3 147:146945	15h 6m 28.96s	-16°33' 36.66"	664.941	814.641	RA:-0.006s DEC:0.144"
3: UCAC3 147:146950	15h 6m 31.97s	-16°35' 12.74"	578.043	979.737	RA:-0.004s DEC:0.422"
4: UCAC3 147:146933	15h 6m 23.12s	-16°35' 18.45"	801.935	1003.774	RA:-0.228s DEC:-0.664"
5: UCAC3 147:146952	15h 6m 33.53s	-16°33' 46.64"	548.531	826.243	RA:0.508s DEC:0.671"
6: UCAC3 147:146955	15h 6m 37.60s	-16°32' 37.12"	451.278	696.080	RA:-0.325s DEC:-0.165"
7: UCAC3 147:146970	15h 6m 41.92s	-16°33' 59.17"	333.266	834.189	RA:0.056s DEC:-0.073"
8: UCAC3 147:146978	15h 6m 45.44s	-16°33' 00.09"	249.979	724.299	RA:-0.082s DEC:-0.350"

TABLE IX: The reference stars used in Figure 7

Date (UT)	JD	RA (hr)	DEC (°)
3 Jul 2014 8:36:56	2456841.9	15h 38m 31.48s	20h 40m 45.72s
17 Jul 2014 5:22:28	2456855.7	15h 12m 04.57s	06h 28m 56.21s
21 Jul 2014 5:28:35	2456859.7	15h 08m 36.74s	12h 03m 19.29s
25 Jul 2014 1:01:55	2456863.5	15h 06m 34.51s	16h 34m 13.59s

TABLE X: Data from observations.

Time (UT and JD)	RA Observed RA Calculated	DEC Observed DEC Calculated
26 Jul 2014 2456841.8	15h 38m 31.48s 15h 38' 43.33"	20°40m 45.72s 20°35' 54.72"

TABLE XI: Comparison of observed and ephemeris generated equatorial coordinates

Reference Star	Magnitude of Star	Magnitude of 2102 Tantalus
UCAC3 222:117955	14.15	16.37
UCAC3 168:137002	15.06	16.79
UCAC3 157:139598	13.19	17.24
UCAC3 147:146955	15.66	17.59

TABLE XII: Photometry

ACKNOWLEDGMENTS

We would like to thank Dr. Michael Faison and Dr. Cassandra Fallscheer for teaching us the theory and techniques used in this research paper. We would also like to express our appreciation for the assistance provided by Andrew Warren, Christine Chang, Daksha Rajagopalan, and James Chang.

REFERENCES

[1] Orbital Elements. Digital image. Wikipedia.org. N.p.,n.d.

[2] JPL. Solar System Dynamics. Horizons Web Interface. FirstGov, n.d. Web. 26 Jul 2014. ¡http://ssd.jpl.nasa.gov/horizons.cgi¿

[3] Meade LX200-ACF. Meade Instruments. Meade Instruments Corp., n.d. Web. 27 July 2014. ¡http://www.meade.com¿

[4] JPL. 2102 Tantalus (1975 YA) Horizons Web Interface. FirstGov, n.d. Web. 08 August 2013. ¡http://ssd.jpl.nasa.gov/sbdb.cgitop¿

[5] Giesen J. "Solving Kepler's Equation." N.p., n.d. Web. 7 Aug. 2013. ¡http://www.jgiesen.de/kepler/kepler.html¿.

[6] STL-1301E Typical Specifications. Santa Barbara Instrument Group, Inc., 20 Aug 2007. Web. 27 Jul 2014. ¡http://www.meade.com¿

[7] USNO. Integrated Image and Catalogue Archive Service, S. Levine, n.d. Web. 27 July 2014. ¡http://www.nofs.navy.mil/data/fchpix/¿.